Donor-controlled photophysics in divinyl-functionalized phenanthroimidazole emitters

Liudmila Loghina[1]*, Jiri Jancalek[1], Zuzana Zmrhalova[1], Roman Jambor[2], Ales Imramovsky[3], Stepan Podzimek[4,5], Zdena Ruzickova[2], and Miroslav Vlcek[1,2]

[1]*Center of Materials and Nanotechnologies, Faculty of Chemical Technology, University of Pardubice, 530 02 Pardubice, Czech Republic.*
[2]*Department of General and Inorganic Chemistry, Faculty of Chemical Technology, University of Pardubice, 532 10 Pardubice, Czech Republic.*
[3]*Institute of Organic Chemistry and Technology, Faculty of Chemical Technology, University of Pardubice, 53210 Pardubice, Czech Republic.*
[4]*Department of Chemistry and Technology of Macromolecular Materials, Faculty of Chemical Technology, University of Pardubice, 532 10 Pardubice, Czech Republic.*
[5]*Synpo, a. s., S. K. Neumanna 1316, 532 07 Pardubice, Czech Republic.*

* Correspondence: liudmila.loghina@upce.cz.

Abstract

The covalent integration of molecular fluorophores into polymer matrices is an attractive strategy for incorporating highly emissive molecular units into processable solid-state materials while retaining their photophysical response and reducing chromophore migration, aggregation, and phase separation. Herein, we report a series of three divinyl-functionalized phenanthro[9,10-*d*]imidazole emitters, PIm-DN-DV, PIm-OMeF-DV, and PIm-PyF-DV, designed to elucidate the influence of donor architecture on both molecular and polymer-integrated photophysics. The monomers were synthesized through modular Debus-Radziszewski condensation and palladium-catalysed Buchwald-Hartwig coupling, followed by incorporation of terminal vinyl groups enabling radical copolymerization with *N*-vinylcarbazole. DFT calculations and cyclic voltammetry revealed systematic donor-controlled stabilization of the HOMO level, with HOMO(CV) values shifting from -5.18 eV for PIm-DN-DV to -5.32 and -5.42 eV for the fluorene-containing PIm-OMeF-DV and PIm-PyF-DV derivatives, respectively. In solution, the final monomers display blue-green emission with PLQY values increasing from 43.3% for PIm-DN-DV to 70.6% and 90.1% for PIm-OMeF-DV and PIm-PyF-DV. Upon copolymerization with *N*-vinylcarbazole, the resulting VK-based films exhibit matrix-defined absorption but retain donor-dependent violet-to-blue emission. Notably, the fluorene-containing copolymer films exhibit highly efficient solid-state photoluminescence with PLQY values of 90.8% and 92.4%, accompanied by fast nanosecond decay dynamics. These results indicate that divinyl-functionalized phenanthroimidazoles are versatile polymerizable emitters and that covalent embedding into a carbazole-rich matrix provides an efficient route to bright donor-tunable emissive films.

Introduction

The development of advanced fluorescent materials remains central to progress in optoelectronics, photonics, bioimaging, sensing, and information-security technologies [1-3]. In

this context, π-conjugated organic molecules with high emission efficiency, tunable photophysical properties, and structural robustness have attracted increasing attention as core components of emissive systems. However, the transfer of strong molecular fluorescence from dilute solution into applicable solid-state materials remains a significant challenge. Physical blending of low-molecular-weight emitters with polymer matrices is synthetically simple, but it may suffer from phase separation, concentration-dependent aggregation, non-uniform chromophore distribution, and gradual emitter migration [4-6]. In contrast, covalent incorporation of fluorescent units into polymer backbones or side-chain architectures offers a more robust strategy, allowing the emissive component to be immobilized while preserving processability, film-forming ability, and material stability [1,4,7].

Fluorescent monomers, which combine intrinsic emission with polymerization capability, have therefore emerged as important building blocks for the construction of light-emitting films, nanostructured materials, sensors, and functional polymer matrices [1,2,7]. Vinyl-functionalized fluorophores are particularly attractive in this respect because they are compatible with radical polymerization and can be directly combined with electronically active vinyl comonomers. This approach enables the preparation of emissive polymers in which the chromophore is not simply dispersed as a guest molecule but chemically incorporated into the macromolecular structure. Such covalent integration can improve film homogeneity, reduce aggregation-related losses, and provide better control over the local environment of the emissive unit [1,4,5,8].

Phenanthro[9,10-*d*]imidazole (PIm) derivatives are well suited for this purpose because their rigid fused aromatic core combines high structural stability, pronounced photoluminescence, and broad synthetic tunability. The imidazole-containing π-conjugated framework allows the construction of donor-π-acceptor and donor-acceptor-donor architectures in which emission colour, excited-state relaxation, charge-transfer contribution, and electronic energy levels can be adjusted by peripheral substitution. Owing to these features, phenanthroimidazole-based compounds have been widely investigated as emitters, host materials, and functional luminophores for OLEDs, light-emitting electrochemical cells, sensors, and other optoelectronic applications [9-13].

Despite this progress, most phenanthroimidazole-based materials have been studied as discrete molecular emitters, dopants, or device-active small molecules, whereas their development as polymerizable monomers remains underexplored. Previous efforts to incorporate fluorescent units into polymerizable or polymer-based emissive systems have mainly focused on established dye and aromatic scaffolds, including perylene diimide derivatives, carbazole-containing polymers, and other conventional organic fluorophores [1,14,15]. In comparison, reports on vinyl-functionalized phenanthroimidazoles remain scarce, despite their favourable photophysical profile and synthetic accessibility. A limited number of examples have demonstrated the feasibility of self-polymerizable phenanthroimidazole monomers and covalently linked PIm/PPI-based stabilizers or emissive units in polymer coatings [16-18].

However, systematic comparison of how different donor fragments affect the photophysics of divinyl-functionalized PIm emitters and their corresponding vinylcarbazole copolymers has not yet been established.

N-Vinylcarbazole was selected as the comonomer because poly(*N*-vinylcarbazole) is a classical photoconductive and hole-transporting polymer widely used in organic optoelectronics, photorefractive materials, light-emitting systems, and photovoltaic devices [19,20]. Its carbazole-rich structure provides a rigid aromatic environment, good film-forming properties, and electronic compatibility with donor-containing fluorescent units. Therefore, copolymerization of divinyl PIm emitters with VK offers a direct route to emissive polymer films in which the chromophore is covalently embedded into a carbazole-based matrix rather than physically dispersed.

In this work, we report a series of three divinyl-functionalized phenanthroimidazole emitters designed to establish a direct link between donor architecture, molecular photophysics, and emission behaviour after covalent integration into an *N*-vinylcarbazole (VK)-based polymer matrix. The series comprises PIm-DN-DV, bearing two naphthylamine donor units, and two fluorene-containing analogues, PIm-OMeF-DV and PIm-PyF-DV, in which methoxyphenyl or pyridyl substitution modulates the electronic character of the phenanthroimidazole fragment. The monomers were synthesized through modular Debus-Radziszewski condensation and Buchwald-Hartwig coupling strategies and subsequently copolymerized with VK at low chromophore loading. This molecular-to-polymer comparison makes it possible to distinguish donor-controlled effects from matrix-induced effects in the solid state. The resulting VK copolymer films retain donor-dependent violet-to-blue emission and, in the case of the fluorene-containing derivatives, exhibit very high solid-state PLQY values above 90%. Thus, the present study demonstrates that divinyl-functionalized PIm emitters provide an effective platform for constructing covalently integrated, highly emissive polymer films with tunable excited-state behaviour.

Experimental

General methods and materials

All chemicals and solvents were obtained from commercial suppliers and used without further purification unless otherwise stated.

The Nuclear Magnetic Resonance (NMR) spectra were recorded from solutions in CDCl3 at 295 K on a Bruker AscendTM 500 spectrometer at frequencies 500.13 MHz for ^{1}H and 125.76 MHz for ^{13}C, respectively. The values of ^{1}H chemical shifts were calibrated to residual signals of $CDCl_3$ (δ (^{1}H) = 7.26 ppm). The values of ^{13}C chemical shifts were referenced to the signals of $CDCl_3$ (δ (^{13}C) = 77.23 ppm). IR spectra in the region 4500-500 cm^{-1} (resolution of 2 cm^{-1}) were measured using a single-bounce diamond ATR crystal on a Vertex 70V FT-IR spectrometer (Bruker, Germany).

Diffraction data were collected using a Bruker Venture D8 diffractometer (Bruker, Germany) at 150 K with graphite-monochromated Mo-Kα (λ = 0.7107 Å) radiation. The frames were integrated with the Bruker SAINT software package using a narrow frame algorithm. Data

were corrected for absorbance effects using the multi-scan method (SADABS). The obtained data were treated using the XT version 2014/5 and SHELXL-2019/1 software, implemented in the APEX4 v2021.10-0 (Bruker AXS) system. All non-hydrogen atoms were refined using anisotropic displacement parameters. Crystallographic data for the structural analyses have been deposited with the Cambridge Crystallographic Data Centre, CCDC nos. 2566697-2566699. Copies of this information may be obtained free of charge from The Director, CCDC, 12 Union Road, Cambridge CB2 1EZ, UK (Fax: +44-1223-336033; e-mail: deposit@ccdc.cam.ac.uk or http://www.ccdc.cam.ac.uk). Elemental analyses were performed on a Flash 2000 CHNS Analyzer (ThermoFisher Scientific). The optical properties were measured using a Fluorometer PTI QuantaMaster 400 (Horiba, Germany) to obtain PL data in the spectral range of 300-850 nm using excitation wavelength λ = 300-350 nm and a UV-3600 (Shimadzu, Japan) spectrometer to get UV-Vis absorbance spectra in the spectral range 200-800 nm. The PL lifetime measurements were performed using TCSPC accessories for Fluorometer PTI QuantaMaster 400 with 390 nm light pulse excitation and the pulse duration < 1.3 ns produced by NanoLED-390 (Horiba Scientific).

Synthetic procedures

Synthesis of intermediate phenanthroimidazoles

1,2-Bis(4-bromophenyl)-1H-phenanthro[9,10-d]imidazole (PIm-Br)

A mixture of 4-bromobenzaldehyde (5.0 g, 27 mmol) and phenanthrene-9,10-dione (5.62 g, 27 mmol) was suspended in glacial acetic acid (120 ml) and stirred until partially dissolved. To this suspension, 4-bromoaniline (9.29 g, 54 mmol) and ammonium acetate (6.24 g, 81 mmol) were added successively under constant stirring. The resulting mixture was heated at reflux for 7 h. Reaction progress was monitored by thin-layer chromatography (TLC) using CH_2Cl_2. Upon cooling to room temperature, the mixture was diluted with water (approximately three times the volume), and the precipitated solid was collected by vacuum filtration, washed thoroughly with water, and then with ethanol. The crude product was air-dried and purified by flash column chromatography on silica gel using CH_2Cl_2 as eluent to afford the target compound as an off-white powder. Yield: 12.37 g (86.7%). Anal. calcd for $C_{27}H_{16}Br_2N_2$ (M_r = 528.25): C, 61.39%; H, 3.05%; Br, 30.25%; N, 5.30%. Found: C, 61.59%; H, 2.99%; Br, 29.72%; N, 5.19%. ^{1}H NMR (500.13 MHz, $CDCl_3$), δ: 8.83 (dd, $^3J_{H,H}$ = 8.0 Hz, $^4J_{H,H}$ = 1.0 Hz, 1H), 8.76 (d, $^3J_{H,H}$ = 8.4 Hz, 1H), 8.69 (d, $^3J_{H,H}$ = 8.4 Hz, 1H), 7.76-7.72 (m, 3H), 7.66 (ddd, $^3J_{H,H}$ = 8.4, 6.9 Hz, $^4J_{H,H}$ = 1.2 Hz, 1H), 7.53 (ddd, $^3J_{H,H}$ = 8.3, 6.9 Hz, $^4J_{H,H}$ = 1.1 Hz, 1H), 7.45 (dt, $^3J_{H,H}$ = 10.6, 2.1 Hz, 2H), 7.40 (dt, $^3J_{H,H}$ = 10.6, 2.0 Hz, 2H), 7.35 (dt, $^3J_{H,H}$ = 11.0, $^4J_{H,H}$ = 2.6 Hz, 2H), 7.2 (ddd, $^3J_{H,H}$ = 8.1, 6.9 Hz, $^4J_{H,H}$ = 0.8 Hz, 1H), 7.19 (d, $^3J_{H,H}$ = 8.3 Hz, 1H). ^{13}C NMR (125.76 MHz, $CDCl_3$), δ: 149.85 (N-C=N), 137.73, 133.73, 131.78, 130.99, 130.77, 129.55, 129.30, 128.49, 128.20, 127.60, 127.15, 126.66, 126.07, 125.39, 124.43, 124.21, 123.77, 123.33, 122.87, 122.85, 120.81.

1-(4-bromophenyl)-2-(2-methoxyphenyl)-1H-phenanthro[9,10-d]imidazole (PIm-BrOMe)

The compound was synthesized via a one-pot condensation of 2-methoxybenzaldehyde (5.0 g, 36.7 mmol), phenanthrene-9,10-dione (7.64 g, 36.7 mmol), 4-bromoaniline (9.48 g, 55 mmol), and ammonium acetate (8.48 g, 110 mmol) in glacial acetic acid (120 ml), using the same conditions as described for PIm-Br. The reaction mixture was heated at reflux for 12 h and worked up by dilution with water, filtration, and washing with water and ethanol. After purification by flash chromatography (CH_2Cl_2), the product was obtained as an off-white solid. Yield: 11.4 g (64%). ^{1}H NMR (500.13 MHz, $CDCl_3$), δ: 8.82-8.85 (d, $^3J_{H,H}$ = 8.27 Hz, 1H), 8.78-8.76 (d, $^3J_{H,H}$ = 8.27 Hz, 1H), 8.71-8.69 (d, $^3J_{H,H}$ = 8.27 Hz, 1H), 7.73 (t, $^3J_{H,H}$ = 7.50 Hz, 1H), 7.64 (dt, $^3J_{H,H}$ = 7.69, $^4J_{H,H}$ = 1.15 Hz, 1H), 7.56-7.55 (d, $^3J_{H,H}$ = 8.46 Hz, 2H), 7.54-7.51 (m, 2H), 7.38-7.26 (m, 5H), 7.01 (t, $^3J_{H,H}$ = 7.45 Hz, 1H), 6.76-6.75 (d, $^3J_{H,H}$ = 8.15 Hz, 1H), 3.54 (s, 3H). ^{13}C NMR (125.76 MHz, $CDCl_3$), δ: 157.50; 149.95; 137.71; 137.48; 132.58; 132.34; 131.56; 130.26; 129.28; 128.27; 127.41; 127.37; 127.29; 126.42; 125.67; 125.08; 124.30; 123.20; 123.07; 122.69; 122.91; 120.93; 120.67; 119.93; 110.68; 55.02.

1-(4-bromophenyl)-2-(pyridin-4-yl)-1H-phenanthro[9,10-d]imidazole (PIm-BrPy)

The compound was prepared by condensation of isonicotinaldehyde (5.0 g, 46.7 mmol), phenanthrene-9,10-dione (9.72 g, 46.7 mmol), 4-bromoaniline (16.07 g, 93.4 mmol), and ammonium acetate (21.6 g, 280 mmol) in glacial acetic acid (180 ml), using the same reaction conditions as described for PIm-Br. The reaction was carried out under reflux for 12 h. After cooling, the mixture was diluted with water, and the resulting precipitate was collected by filtration, washed thoroughly with water and ethanol, and dried in air. The crude solid was purified by column chromatography on silica gel using CH_2Cl_2 as eluent to afford the product as an off-white solid. Yield: 18.1 g (86%). ^{1}H NMR (500.13 MHz, $CDCl_3$), δ: 8.83-8.81 (d, $^3J_{H,H}$ = 8.33 Hz, 1H), 8.76-8.74 (d, $^3J_{H,H}$ = 8.33 Hz, 1H), 8.68-8.66 (d, $^3J_{H,H}$ = 8.33 Hz, 1H), 8.57-8.56 (d, $^3J_{H,H}$ = 6.25 Hz, 2H), 7.79-7.77 (d, $^3J_{H,H}$ = 8.54 Hz, 2H), 7.75 (t, $^3J_{H,H}$ = 7.50 Hz, 1H), 7.66 (t, $^3J_{H,H}$ = 7.71 Hz, 1H), 7.55 (t, $^3J_{H,H}$ = 7.50 Hz, 1H), 7.45-7.44 (d, $^3J_{H,H}$ = 6.04 Hz, 1H), 7.40-7.38 (d, $^3J_{H,H}$ = 8.33 Hz, 2H), 7.32 (t, $^3J_{H,H}$ = 7.50 Hz, 1H), 7.18-7.16 (d, $^3J_{H,H}$ = 8.33 Hz, 1H). ^{13}C NMR (125.76 MHz, $CDCl_3$), δ: 175.08; 149.57; 147.43; 138.16; 137.98; 137.33; 134.03; 130.56; 129.92; 128.90; 128.64; 127.77; 126.98; 126.81; 126.41; 125.89; 124.75; 124.49; 123.37; 123.15; 122.89; 122.64; 120.94.

Buchwald-Hartwig amination and donor introduction

N,N'-((1H-phenanthro[9,10-d]imidazole-1,2-diyl)bis(4,1-phenylene))bis(naphthalen-1-amine) (PIm-DN)

Tris(dibenzylideneacetone)dipalladium(0) ($Pd_2(dba)_3$, 1.14 g, 1.25 mmol) and 1,1'-bis(diphenylphosphino)ferrocene (dppf, 1.39 g, 2.50 mmol) were added to dry, degassed toluene (120 ml) under an argon atmosphere. The mixture was stirred at room temperature for 10 min, followed by the addition of PIm-Br (10.0 g, 18.9 mmol), 1-naphthylamine (5.96 g, 41.6 mmol), and sodium tert-butoxide (8.0 g, 83.2 mmol). The reaction mixture was degassed by several freeze-pump-thaw cycles and refluxed under argon for 15 h. Reaction progress was monitored by TLC

($CHCl_3$ with 5% EtOAc). After cooling to room temperature, the mixture was diluted with an equal volume of $CHCl_3$ and filtered through a short silica gel pad, eluting with additional $CHCl_3$. The combined organic fractions were concentrated under reduced pressure, and the crude product was purified by column chromatography on silica gel ($CHCl_3$ with 5% EtOAc), affording the product as a pale yellow crystalline solid. Yield: 9.8 g (80%). ^{1}H NMR (500.13 MHz, $CDCl_3$), δ: 8.96-8.98 (d, $^3J_{H,H}$ = 7.53 Hz, 1H), 8.75-8.74 (d, $^3J_{H,H}$ = 8.32 Hz, 1H), 8.68-8.67 (d, $^3J_{H,H}$ = 8.32 Hz, 1H), 8.05-8.03 (d, $^3J_{H,H}$ = 8.32 Hz, 1H), 7.98-7.96 (d, $^3J_{H,H}$ = 8.32 Hz, 1H), 7.88-7.87 (d, $^3J_{H,H}$ = 8.18 Hz, 1H), 7.85-7.83 (d, $^3J_{H,H}$ = 8.18 Hz, 1H), 7.72 (t, $^3J_{H,H}$ = 7.50 Hz, 1H), 7.65 (t, $^3J_{H,H}$ = 9.28 Hz, 2H), 7.60 (t, $^3J_{H,H}$ = 5.18 Hz, 1H), 7.56-7.33 (m, 13H), 7.26-7.24 (m, 2H), 7.05-7.03 (d, $^3J_{H,H}$ = 8.37 Hz, 2H), 6.87-6.86 (d, $^3J_{H,H}$ = 8.37 Hz, 2H), 6.37 (s, 1H), 6.22 (s, NH). ^{13}C NMR (125.76 MHz, $CDCl_3$), δ: 151.23; 146.87; 146.45; 137.58; 137.36; 134.97; 134.84; 130.95; 129.97; 129.30; 128.82; 128.69; 128.65; 128.61; 128.41; 127.97; 127.50; 126.50; 125.83; 125.01; 124.88; 124.34; 124.21; 123.22; 122.39; 122.31; 121.11; 118.89; 118.39; 116.95; 115.73.

N-(4-(2-(2-methoxyphenyl)-1H-phenanthro[9,10-d]imidazol-1-yl)phenyl)-3-methylaniline (PIm-OMeTol)

Tris(dibenzylideneacetone)dipalladium(0) ($Pd_2(dba)_3$, 0.38 g, 0.417 mmol) and RuPhos (2-Dicyclohexylphosphino-2',6'-diisopropoxybiphenyl, 0.39 g, 0.834 mmol) were added to dry, degassed toluene (60 ml) under argon. The mixture was stirred at room temperature for 10 min to allow preformation of the active catalytic species. Subsequently, PIm-BrOMe (4.0 g, 8.34 mmol), m-toluidine (0.94 ml, 8.8 mmol), and sodium *tert*-butoxide (1.6 g, 16.7 mmol) were added. The reaction mixture was further degassed by bubbling of Ar and then heated under reflux for 6 h. Reaction progress was monitored by TLC ($CHCl_3$ with 5% EtOAc). After completion, the mixture was cooled, diluted with chloroform, and filtered through a short silica gel pad. The crude product was purified by column chromatography ($CHCl_3$ with 5% EtOAc) to afford the target compound as a beige crystalline solid. Yield: 4.1 g (97%). ^{1}H NMR (500.13 MHz, $CDCl_3$), δ: 8.91-8.89 (d, $^3J_{H,H}$ = 7.82 Hz, 1H), 8.81-8.79 (d, $^3J_{H,H}$ = 8.56 Hz, 1H), 8.74-8.72 (d, $^3J_{H,H}$ = 8.56 Hz, 1H), 7.73 (t, $^3J_{H,H}$ = 7.30 Hz, 1H), 7.66 (t, $^3J_{H,H}$ = 7.30 Hz, 1H), 7.55-7.51 (m, 3H), 7.39-7.34 (q, $^3J_{H,H}$ = 16.56, 7.30 Hz, 2H), 7.25-7.23 (d, $^3J_{H,H}$ = 8.77 Hz, 3H), 7.21-7.20 (d, $^3J_{H,H}$ = 7.79 Hz, 1H), 7.05-7.03 (d, $^3J_{H,H}$ = 8.77 Hz, 2H), 7.01-6.96 (q, $^3J_{H,H}$ = 17.05, 7.79 Hz, 2H), 6.92 (s, 1H), 6.85-6.84 (d, $^3J_{H,H}$ = 7.30 Hz, 1H), 6.80-6.78 (d, $^3J_{H,H}$ = 7.79 Hz, 1H), 6.13 (s, 1H), 3.60 (s, 3H), 2.34 (s, 3H). ^{13}C NMR (125.76 MHz, $CDCl_3$), δ: 157.73; 150.30; 144.31; 141.80; 139.38; 137.13; 132.47; 131.11; 129.78; 129.33; 129.26; 129.09; 128.11; 127.67; 127.40; 127.20; 126.26; 125.32; 124.79; 124.04; 123.25; 123.11; 123.02; 122.83; 121.10; 120.31; 119.90; 116.17; 110.54; 55.03; 21.58.

3-methyl-N-(4-(2-(pyridin-4-yl)-1H-phenanthro[9,10-d]imidazol-1-yl)phenyl)aniline (PIm-PyTol)

Tris(dibenzylideneacetone)dipalladium(0) ($Pd_2(dba)_3$, 0.41 g, 0.448 mmol) and RuPhos (2-Dicyclohexylphosphino-2',6'-diisopropoxybiphenyl, 0.42 g, 0.900 mmol) were dissolved in dry,

degassed toluene (60 ml) under an argon atmosphere and stirred at room temperature for 10 min. PIm-BrPy (4.0 g, 8.9 mmol), m-toluidine (1.05 ml, 9.8 mmol), and sodium *tert*-butoxide (1.71 g, 17.8 mmol) were then added. The mixture was further degassed and refluxed under argon for 6 h. Reaction progress was monitored by TLC ($CHCl_3$ with 15% EtOAc). After cooling, the mixture was diluted with chloroform and filtered through a short silica gel pad. The crude product was purified by column chromatography ($CHCl_3$ with 15% EtOAc), affording the desired compound as a beige solid. Yield: 4.05 g (95%). ^{1}H NMR (500.13 MHz, $CDCl_3$), δ: 8.96-8.87 (d, $^3J_{H,H}$ = 7.81 Hz, 1H), 8.77-8.75 (d, $^3J_{H,H}$ = 8.15 Hz, 1H), 8.70-8.68 (d, $^3J_{H,H}$ = 8.15 Hz, 1H), 8.59-8.58 (d, $^3J_{H,H}$ = 6.11 Hz, 2H), 7.75 (t, $^3J_{H,H}$ = 7.47 Hz, 1H), 7.66 (t, $^3J_{H,H}$ = 7.47 Hz, 1H), 7.58-7.53 (m, 3H), 7.43-7.42 (d, $^3J_{H,H}$ = 8.15 Hz, 1H), 7.53 (t, $^3J_{H,H}$ = 7.47 Hz, 1H), 7.32-7.31 (d, $^3J_{H,H}$ = 8.15 Hz, 2H), 7.26 (t, $^3J_{H,H}$ = 3.85 Hz, 1H), 7.21-7.19 (d, $^3J_{H,H}$ = 8.70 Hz, 2H), 7.08-7.05 (m, 2H), 6.92-6.91 (d, $^3J_{H,H}$ = 7.43 Hz, 1H), 6.25 (s, NH). ^{13}C NMR (125.76 MHz, $CDCl_3$), δ: 149.98; 147.93; 145.80; 141.29; 139.75; 138.25; 137.69; 129.78; 129.70; 129.57; 129.38; 129.33; 128.57; 127.59; 127.24; 126.65; 126.08; 125.58; 124.29; 123.97; 123.34; 123.15; 123.00; 122.80; 121.29; 120.81; 117.13; 116.96; 21.72.

Divinyl-functionalized compounds

2-bromo-9,9-bis(4-vinylbenzyl)-9H-fluorene (F-DVB)

To a stirred solution of sodium hydroxide (13.52 g, 338 mmol) in distilled water (15 ml) was added dimethyl sulfoxide (100 ml), followed by 2-bromofluorene (15.0 g, 61 mmol) and tetraethylammonium bromide (0.5 g) as a phase-transfer catalyst. The mixture was stirred at room temperature for 20 min, then 4-vinylbenzyl chloride (19.0 ml, 135 mmol) was added in five portions. The reaction was mildly exothermic and was stirred at room temperature for 8 h. Reaction progress was monitored by TLC (petroleum ether with 10% CH_2Cl_2). Upon completion, the reaction mixture was poured into water (1 l) and extracted with diethyl ether (3 × 100 ml). The combined organic layers were washed with brine, dried over anhydrous sodium sulfate, and concentrated under reduced pressure. The crude product was purified by column chromatography on silica gel (petroleum ether with 10% CH_2Cl_2), affording the target compound as a viscous colourless liquid. Yield: 22.3 g (76%). ^{1}H NMR (500.13 MHz, $CDCl_3$), δ: 7.62 (d, $^4J_{H,H}$ = 1.50 Hz, 1H), 7.47-7.45 (d, $^3J_{H,H}$ = 7.54 Hz, 1H), 7.42-7.35 (m, 3H), 7.30-7.28 (m, 2H), 7.00-7.04 (d, $^3J_{H,H}$ = 8.21 Hz, 4H), 6.68-6.66 (d, $^3J_{H,H}$ = 8.21 Hz, 4H), 6.60-6.55 (dd, $^3J_{H,H}$ = 17.60, 10.89 Hz, 2H), 5.64-5.61 (d, $^3J_{H,H}$ = 17.60 Hz, 2H), 5.33 (s, 1H), 5.16-5.14 (d, $^3J_{H,H}$ = 10.89 Hz, 2H), 3.42-3.34 (q, $^3J_{H,H}$ = 22.79, 13.07 Hz, 4H). ^{13}C NMR (125.76 MHz, $CDCl_3$), δ: 150.55; 147.92; 140.07; 140.03; 136.72; 136.50; 135.40; 130.50; 130.35; 127.88; 127.49; 126.93; 125.34; 124.78; 121.39; 120.24; 120.14; 113.21; 87.11; 53.64; 45.25.

N,N'-((1H-phenanthro[9,10-d]imidazole-1,2-diyl)bis(4,1-phenylene))bis(N-(4-vinylphenyl)naphthalen-1-amine) (PIm-DN-DV)

PIm-DN (3.0 g, 4.6 mmol), 1-bromo-4-vinylbenzene (2.0 g, 11.04 mmol), sodium tert-butoxide (1.32 g, 13.8 mmol), tris(dibenzylideneacetone)dipalladium(0) ($Pd_2(dba)_3$, 0.13 g, 0.138 mmol), and 1,1′-bis(diphenylphosphino)ferrocene (dppf, 0.153 g, 0.276 mmol) were combined in dry toluene (50 ml) under argon. The mixture was stirred under reflux for 18 h. Reaction progress was monitored by TLC ($CHCl_3$). After cooling to room temperature, the reaction mixture was diluted with chloroform and directly loaded onto a silica gel column. The product was purified by flash chromatography using chloroform as eluent, affording the target compound as a yellowish amorphous solid. Yield: 2.8 g (71%). Anal. calcd for $C_{63}H_{44}N_4$ (M_r = 857.07): C, 88.29; H, 5.17; N, 6.54. Found: C, 88.13%; H, 5.04%; N, 6.26%. ^{1}H NMR (500.13 MHz, $CDCl_3$), δ: 8.80-8.78 (d, $^3J_{H,H}$ = 7.69 Hz, 1H), 8.71-8.69 (d, $^3J_{H,H}$ = 8.37 Hz, 1H), 8.63-8.62 (d, $^3J_{H,H}$ = 8.37 Hz, 1H), 7.88-7.75 (m, 6H), 7.65 (t, $^3J_{H,H}$ = 7.69 Hz, 1H), 7.56 (t, $^3J_{H,H}$ = 8.37 Hz, 1H), 7.49-7.38 (m, 8H), 7.35-7.25 (m, 10H), 7.08-7.02 (m, 7H), 6.90-6.88 (d, $^3J_{H,H}$ = 8.89 Hz, 2H), 6.65-6.59 (dd, $^3J_{H,H}$ = 10.77, 17.44 Hz, 2H), 5.63-5.58 (dd, $^3J_{H,H}$ = 4.10, 17.61 Hz, 2H), 5.15-5.11 (dd, $^3J_{H,H}$ = 8.54, 10.94 Hz, 2H). ^{13}C NMR (125.76 MHz, $CDCl_3$), δ: 150.93; 149.01; 148.56; 147.22; 147.04; 142.77; 142.52; 137.14; 136.10; 136.00; 135.34; 135.26; 132.43; 131.92; 131.37; 131.02; 130.63; 130.07; 130.02; 129.73; 129.00; 128.60; 128.44; 128.06; 128.01; 127.32; 127.24; 127.21; 127.15; 127.10; 127.03; 126.91; 126.59; 126.45; 126.38; 126.32; 126.11; 125.33; 124.54; 124.10; 124.02; 123.75; 123.21; 123.13; 123.00; 122.78; 122.63; 122.60; 121.39; 120.78; 120.20; 112.63; 112.29.

N-(4-(2-(2-methoxyphenyl)-1H-phenanthro[9,10-d]imidazol-1-yl)phenyl)-N-(m-tolyl)-9,9-bis(4-vinylbenzyl)-9H-fluoren-2-amine (PIm-OMeF-DV)

PIm-OMeTol (3.0 g, 6.0 mmol), F-DVB (3.43 g, 7.2 mmol), sodium tert-butoxide (1.73 g, 18.0 mmol), tris(dibenzylideneacetone)dipalladium(0) ($Pd_2(dba)_3$, 0.27 g, 0.300 mmol), and RuPhos (2-Dicyclohexylphosphino-2′,6′-diisopropoxybiphenyl, 0.28 g, 0.600 mmol) were added to dry toluene (60 ml) under an argon atmosphere. The reaction mixture was heated to reflux and stirred for 20 h. Reaction progress was monitored by TLC ($CHCl_3$). After cooling, the mixture was diluted with chloroform and filtered through a short silica gel pad. The crude residue was purified by column chromatography on silica gel using chloroform as eluent. The target compound was obtained as a beige amorphous solid. Yield: 2.3 g (43%). Anal. calcd for $C_{66}H_{51}N_3O$ (M_r = 902.15): C, 87.87; H, 5.70; N, 4.66; O, 1.77%. Found: C, 87.84%; H, 5.69%; N, 4.48%. ^{1}H NMR (500.13 MHz, $CDCl_3$), δ: 8.89 (s, 1H), 8.76-8.75 (d, $^3J_{H,H}$ = 8.36 Hz, 1H), 8.68-8.67 (d, $^3J_{H,H}$ = 8.36 Hz, 1H), 7.69 (t, $^3J_{H,H}$ = 7.31 Hz, 1H), 7.59 (t, $^3J_{H,H}$ = 9.00 Hz, 2H), 7.54-7.46 (m, 3H), 7.39 (t, $^3J_{H,H}$ = 7.31 Hz, 1H), 7.37-7.20 (m, 8H), 7.08 (d, $^4J_{H,H}$ = 1.75 Hz, 1H), 7.00-6.87 (m, 11H), 6.79-6.77 (d, $^3J_{H,H}$ = 8.05 Hz, 1H), 6.52-6.51 (d, $^3J_{H,H}$ = 8.05 Hz, 4H), 6.47-6.41 (dd, $^3J_{H,H}$ = 17.93, 10.93 Hz, 2H), 5.50-5.46 (d, $^3J_{H,H}$ = 17.93 Hz, 2H), 5.03-5.01 (d, $^3J_{H,H}$ = 10.24 Hz, 2H), 3.58 (s, 3H), 3.33-3.31 (d, $^3J_{H,H}$ = 13.18 Hz, 2H), 3.19-3.16 (d, $^3J_{H,H}$ = 13.18 Hz, 2H), 2.32 (s, 3H). ^{13}C NMR (125.76 MHz, $CDCl_3$), δ: 157.71; 149.51; 148.23; 147.25; 145.45; 140.57; 139.22; 137.45; 136.57; 136.46; 135.09; 132.52; 130.29; 129.17; 128.99; 128.11; 127.35; 127.31; 126.17; 125.41; 124.92; 124.77; 124.26; 124.18; 124.09; 123.02;

122.79; 121.86; 121.30; 121.03; 120.83; 120.39; 119.56; 112.95; 110.46; 56.90; 55.06; 45.23; 21.60.

N-(4-(2-(pyridin-4-yl)-1H-phenanthro[9,10-d]imidazol-1-yl)phenyl)-N-(m-tolyl)-9,9-bis(4-vinylbenzyl)-9H-fluoren-2-amine (PIm-PyF-DV)

PIm-PyTol (3.0 g, 6.3 mmol), F-DVB (3.6 g, 7.5 mmol), sodium tert-butoxide (1.83 g, 18.9 mmol), tris(dibenzylideneacetone)dipalladium(0) ($Pd_2(dba)_3$, 0.29 g, 0.315 mmol), and RuPhos (0.29 g, 0.630 mmol) were added to dry toluene (60 ml) under argon. The reaction mixture was heated at reflux for 18 hours. Reaction progress was monitored by TLC ($CHCl_3$). After cooling, the mixture was diluted with chloroform and filtered through a short pad of silica gel. The crude residue was purified by flash chromatography with chloroform as the eluent, affording a beige amorphous solid. Yield: 2.5 g (45%). Anal. calcd for $C_{64}H_{48}N_4$ (M_r = 873.12): C, 88.04; H, 5.54; N, 6.42. Found: C, 86.83%; H, 5.21%; N, 6.14%. ^{1}H NMR (500.13 MHz, $CDCl_3$), δ: 8.83-8.82 (d, $^3J_{H,H}$ = 7.91 Hz, 1H), 8.75-8.73 (d, $^3J_{H,H}$ = 8.49 Hz, 1H), 8.67-8.65 (d, $^3J_{H,H}$ = 8.49 Hz, 1H), 8.60-8.59 (d, $^3J_{H,H}$ = 4.54 Hz, 2H), 7.71 (t, $^3J_{H,H}$ = 7.66 Hz, 1H), 7.62 (t, $^3J_{H,H}$ = 7.66 Hz, 1H), 7.59-7.58 (d, $^3J_{H,H}$ = 5.74 Hz, 2H), 7.54 (t, $^3J_{H,H}$ = 7.66 Hz, 1H), 7.50 (t, $^3J_{H,H}$ = 8.81 Hz, 2H), 7.40 (t, $^3J_{H,H}$ = 7.66 Hz, 1H), 7.35-7.34 (d, $^3J_{H,H}$ = 8.04 Hz, 2H), 7.30-7.28 (m, 4H), 7.23 (t, $^3J_{H,H}$ = 7.37 Hz, 1H), 7.22-7.21 (m, 1H), 7.16-7.14 (d, $^3J_{H,H}$ = 8.81 Hz, 2H), 7.07-7.05 (m, 3H), 6.98-6.97 (d, $^3J_{H,H}$ = 7.37 Hz, 1H), 6.89-6.87 (d, $^3J_{H,H}$ = 7.74 Hz, 4H), 6.55-6.54 (d, $^3J_{H,H}$ = 7.74 Hz, 4H), 6.45-6.40 (m, 2H), 5.48-5.44 (d, $^3J_{H,H}$ = 17.71 Hz, 2H), 5.01-4.99 (d, $^3J_{H,H}$ = 11.06 Hz, 2H), 3.35-3.32 (d, $^3J_{H,H}$ = 13.28 Hz, 2H), 3.25-3.22 (d, $^3J_{H,H}$ = 13.28 Hz, 2H), 2.37 (s, 3H). ^{13}C NMR (125.76 MHz, $CDCl_3$), δ: 149.79; 149.73; 148.38; 146.88; 145.10; 140.44; 139.50; 138.09; 137.95; 136.56; 136.43; 135.11; 130.26; 130.19; 129.67; 129.38; 129.25; 128.39; 127.45; 127.36; 127.06; 126.41; 126.33; 125.94; 125.67; 125.45; 125.33; 124.96; 124.83; 124.26; 124.21; 123.24; 123.16; 122.95; 122.92; 122.64; 122.21; 121.84; 121.07; 121.04; 119.67; 112.97; 56.95; 45.23; 21.65.

Radical Copolymerization

Radical copolymerization of the three phenanthroimidazole-based divinyl monomers was performed under identical conditions. Each monomer (0.10 g, 5 wt.%) was reacted with *N*-vinylcarbazole (2.0 g, 10.6 mmol) in dry 1,2-dichlorobenzene (12 ml) using azobisisobutyronitrile (AIBN, 0.03 g, 0.18 mmol) as a radical initiator. The mixture was degassed through three freeze-pump-thaw cycles, backfilled with argon, sealed, and stirred at 75 °C for 48 hours. After cooling to room temperature, the reaction mixture was poured into hexane (100 ml). The resulting precipitate was filtered, thoroughly washed with hexane, and dried under vacuum. The copolymers obtained appeared as off-white powders: Poly(PIm-DN-DV-*co*-VK): yield 1.9 g; Poly(PIm-OMeF-DV-*co*-VK): yield 2.0 g; Poly(PIm-PyF-DV-co-VK): yield 1.8 g.

Results and discussion

Molecular design and synthesis

The molecular design of the present series was based on the combination of a phenanthro[9,10-*d*]imidazole emissive core, electronically distinct donor fragments, and terminal vinyl groups enabling radical copolymerization. Phenanthroimidazole was selected as a synthetically accessible and photophysically tunable scaffold, commonly obtained through Debus-Radziszewski-type condensation of phenanthrene-9,10-dione, an aldehyde, an aniline derivative, and ammonium acetate [21]. This multicomponent approach allows independent modification of the N1- and C2-substituents and therefore provides a convenient entry to donor-modified PIm emitters [22].

Three synthetic branches were developed to access structurally related but electronically different divinyl-functionalized monomers. PIm-DN-DV contains two naphthylamine donor fragments attached to the PIm core. In contrast, PIm-OMeF-DV and PIm-PyF-DV combine a PIm acceptor-type fragment with a fluorene-based diarylamine donor bearing two vinylbenzyl termini. The methoxyphenyl and pyridyl substituents were introduced to modulate the electronic character of the PIm fragment while retaining the same polymerizable fluorene-vinylbenzyl unit.

The target compounds were synthesized through a modular sequence involving Debus-Radziszewski condensation, palladium-catalysed Buchwald-Hartwig amination [23], and final donor/vinyl-functional fragment introduction. This strategy enabled the preparation of both final divinyl monomers and intermediate PIm derivatives, allowing the influence of stepwise structural modification on optical behaviour to be evaluated.

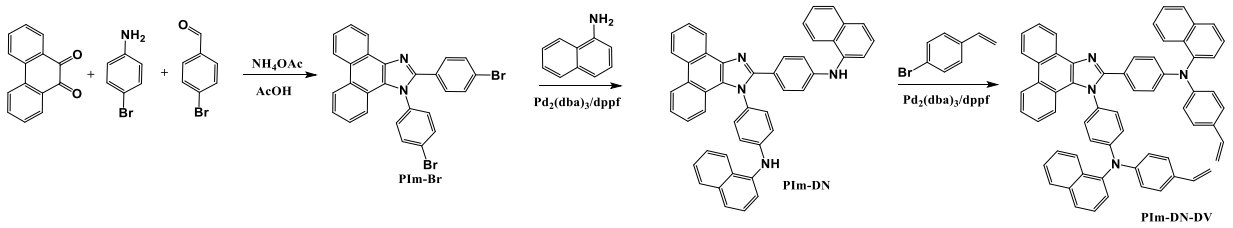

Scheme 1. Synthetic routes of PIm-DN-DV

In the second step, the Buchwald-Hartwig amination of PIm-Br with 1-naphthylamine, using $Pd_2(dba)_3$ and dppf as the catalytic system, produces the diarylamine derivative (PIm-DN) [24]. This intermediate is a symmetrical bis(diarylamine), containing two naphthylamine units linked through para-substituted phenylene groups. The final C-N coupling was performed between PIm-DN and 4-vinylbromobenzene using $Pd_2(dba)_3$/dppf as the catalyst to afford the divinyl-functionalized product PIm-DN-DV.

The second synthetic route is outlined in Scheme 2. In the first step, the Debus-Radziszewski condensation of phenanthrene-9,10-dione, 4-bromoaniline, and 2-methoxybenzaldehyde in glacial acetic acid yields the bromo-functionalized intermediate PIm-BrOMe.

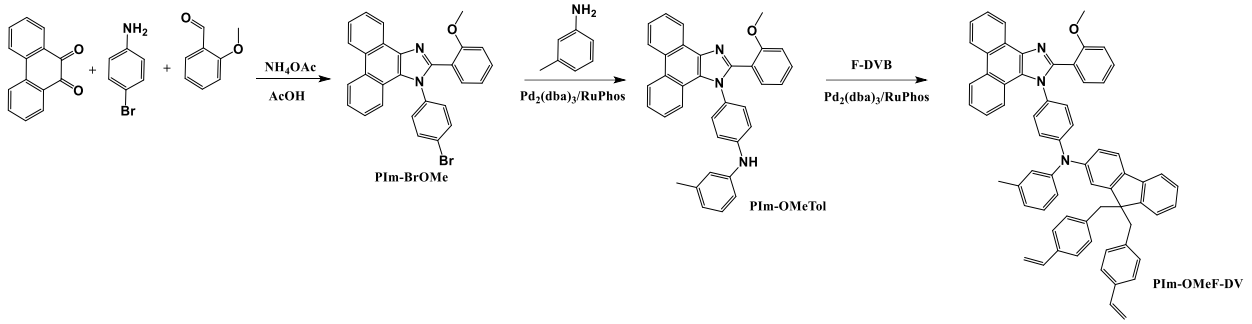

Scheme 2. Synthetic routes of PIm-OMeF-DV

This compound undergoes Buchwald-Hartwig amination with m-toluidine (3-methylaniline) using $Pd_2(dba)_3$ and RuPhos in dry toluene, resulting in the methoxy-substituted monoarylamine derivative PIm-OMeTol. In the final step, this intermediate reacts with F-DVB (2-bromo-9,9-bis(4-vinylbenzyl)-9H-fluorene) under $Pd_2(dba)_3$/RuPhos catalysis, leading to the formation of PIm-OMeF-DV, which features a donor-acceptor-donor structure with terminal vinyl groups suitable for polymerization.

The third synthetic route is depicted in Scheme 3. The Debus-Radziszewski condensation of phenanthrene-9,10-dione, 4-bromoaniline, and isonicotinaldehyde in glacial acetic acid gives the brominated pyridyl-substituted intermediate PIm-BrPy.

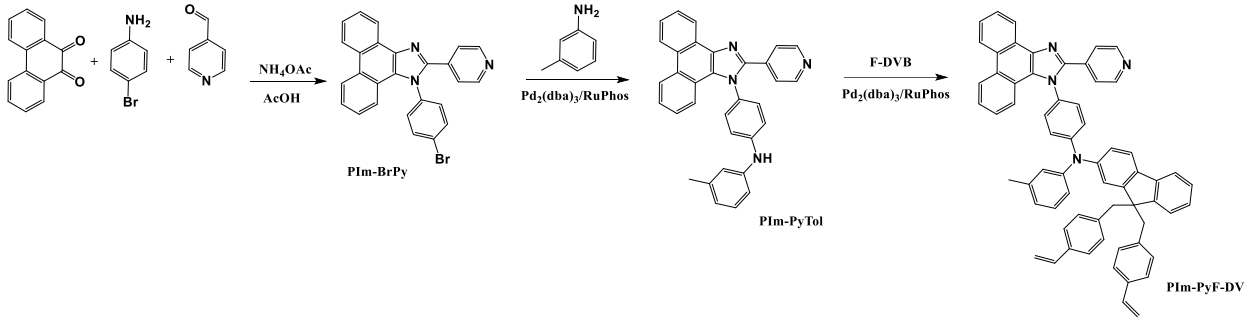

Scheme 3. Synthetic routes of PIm-PyF-DV

Subsequent Buchwald-Hartwig amination with m-toluidine in the presence of $Pd_2(dba)_3$ and RuPhos yields the corresponding monoarylamine PIm-PyTol, which integrates both electron-rich and electron-deficient functionalities. Finally, the C-N coupling with F-DVB under $Pd_2(dba)_3$/RuPhos catalysis affords PIm-PyF-DV. This product combines the structural rigidity of the phenanthroimidazole core with donor-acceptor characteristics and polymerizable vinyl termini.

The three divinyl-functionalized monomers PIm-DN-DV, PIm-OMeF-DV, and PIm-PyF-DV were subjected to free-radical copolymerization with *N*-vinylcarbazole (VK), yielding hybrid copolymers incorporating both emissive fluorophore units and a well-established hole-transporting polymer matrix. Each monomer was introduced at a 5 wt.% ratio with respect to VK

under otherwise identical polymerization conditions. The reactions were carried out in 1,2-dichlorobenzene at 75 °C for 48 hours using azobisisobutyronitrile (AIBN) as the radical initiator. All three copolymers were isolated as light brown powders after precipitation in hexane and exhibited good solubility in chlorinated solvents such as chloroform. The successful formation of the copolymers was confirmed by their solubility profiles and subsequent characterization. Notably, the introduction of extended π-conjugated monomers with functional termini into the polymer matrix provides access to materials with modulated emission and enhanced processability. These hybrid materials combine the photophysical features of the emissive monomers with the mechanical robustness and film-forming properties of the poly(vinylcarbazole) backbone, making them well-suited for spin-coating techniques and further optoelectronic evaluation.

Structural and electronic characterization of the divinyl PIm monomers

The structures of all intermediates and final divinyl-functionalized phenanthroimidazole monomers were confirmed by ^{1}H and $^{13}C\{^{1}H\}$ NMR spectroscopy. The spectra are consistent with the stepwise formation of the phenanthro[9,10-*d*]imidazole core, subsequent donor introduction through Buchwald-Hartwig amination, and final installation of the vinyl-functional fragments. For the bromo-substituted PIm precursors, the diagnostic aromatic signals of the phenanthroimidazole framework were observed in the downfield region, together with substituent-specific resonances such as the methoxy signal for PIm-BrOMe and the pyridyl proton signals for PIm-BrPy. After donor introduction, the appearance of additional arylamine resonances and, where applicable, NH signals confirmed the formation of the corresponding amine intermediates PIm-DN (δ6.22), PIm-OMeTol (δ6.13), and PIm-PyTol (δ6.25).

For the final divinyl monomers, the most important spectral evidence is the presence of terminal vinyl groups. In PIm-DN-DV, vinyl resonances appear as the characteristic pattern in the regions of ca. 6.65-6.59, 5.63-5.58, and 5.15-5.11 ppm. Similar diagnostic vinyl signals are observed for PIm-OMeF-DV at ca. 6.47-6.41, 5.50-5.46, and 5.03-5.01 ppm, and for PIm-PyF-DV at ca. 6.45-6.40, 5.48-5.44, and 5.01-4.99 ppm. The assignments of these resonances are further supported by the 2D NMR data (Figures S15, S18, S19, and S22). The HSQC spectra show the expected one-bond correlations between the vinyl proton resonances and protonated sp^2 carbons, while the COSY spectrum of PIm-OMeF-DV confirms the corresponding proton-proton coupling pattern in the terminal vinyl groups. Together, these correlations support the assignment of the characteristic vinyl resonances and confirm retention of the polymerizable termini after the final coupling step. In the fluorene-containing derivatives, the benzylic CH_2 protons of the 9,9-bis(4-vinylbenzyl)fluorene fragment are also clearly observed as two doublets around 3.3-3.2 ppm, further supporting successful incorporation of the divinyl fluorene donor unit.

The $^{13}C\{^{1}H\}$ and ^{1}H-^{13}C-HSQC NMR spectra further support the assigned structures by showing the expected imidazole C=N carbon resonance around 149-151 ppm, multiple aromatic carbon resonances across the 110-150 ppm region, and substituent-specific aliphatic signals, including methoxy, methyl, fluorene C-9, and benzylic CH_2 carbons where appropriate. Taken together with elemental analysis, the NMR data confirm the successful preparation of the designed intermediates and final divinyl PIm monomers. Full ^{1}H and ^{13}C NMR spectra are provided in the *Supplementary Information*.

The bromo-functionalized intermediates PIm-BrOMe and pyridyl-substituted PIm-BrPy were characterized by single-crystal X-ray diffraction. Single crystals of PIm-BrOMe and PIm-BrPy·CH_3COOH were grown from the $CHCl_3$/EtOH mixture by slow evaporation of solvent from saturated solutions of the parent compounds.

Molecular structures are depicted in Figure 1. The imidazole ring of PIm-BrPy contains C1-N2 (1.323(2) Å) and C2-C3 (1.380(2) Å) double bonds (Σd_{cov} = 1.27 Å and 1.34 Å), while remaining C-N distances are prolonged with the range of 1.378(2) - 1.391(2) Å. The C7 and C12 atoms are below and above the plane defined by the imidazole ring with 0.385 Å and 0.345 Å, demonstrating a non-planar phenanthroimidazole framework. A similar situation was observed in PIm-BrOme, where the imidazole ring contains C1-N2 (1.315(2) Å) and C2-C3 (1.380(2) Å) double bonds (Σd_{cov} = 1.27 Å and 1.34 Å). The remaining C-N distances of the central ring are prolonged with the range of 1.377(2) - 1.3923(18) Å. The non-planar phenanthroimidazole framework is demonstrated by C7 and C12 atoms being 0.382 Å and 0.231 Å out of the plane defined by the imidazole ring.

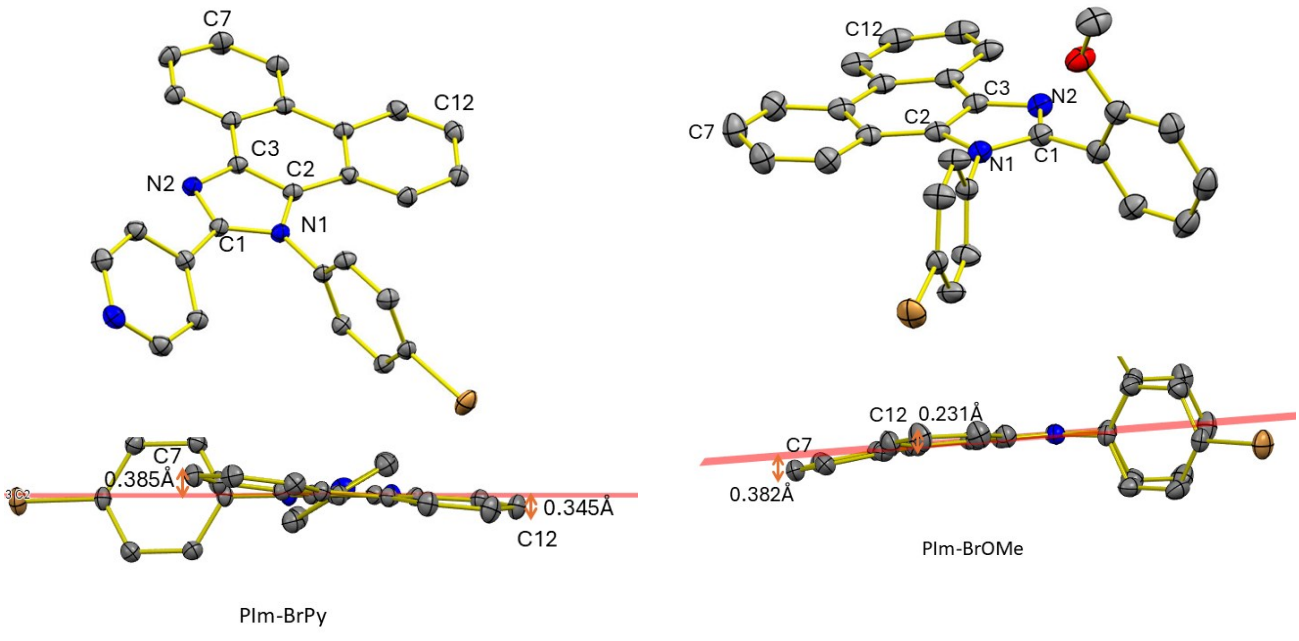

Figure 1. PovRay presentation of PIm-BrPy and PIm-BrOMe. Hydrogen atoms and the molecule of CH_3COOH were omitted for clarity.

Successful Buchwald-Hartwig amination of PIm-BrPy with m-toluidine provided the corresponding monoarylamine PIm-PyTol, whose molecular structure was characterized by single-crystal X-ray diffraction (Figure 2). Single crystals of PIm-PyTol·CH_3CH_2OH were grown from saturated CH_3CH_2OH solution by slow evaporation of the solvent. The molecular structure is depicted in Figure 2 and reveals the presence of a new C24-N3 single bond (1.4022(15) Å) and the absence of the bromide atom. The imidazole ring of PIm-PyTol contains C1-N2 (1.3243(15) Å) and C2-C3 (1.381(2) Å) double bonds (Σd_{cov} = 1.27 Å and 1.34 Å), while remaining C-N distances define single bonds. The non-planar phenanthroimidazole framework is twisted peripherally with the m-toluidine group, with torsion angle N1, N2, N3, C27 at 56.31°, which should reduce excessive π-π stacking of the planar phenanthroimidazoles and can be relevant to the solid-state emission behaviour [9].

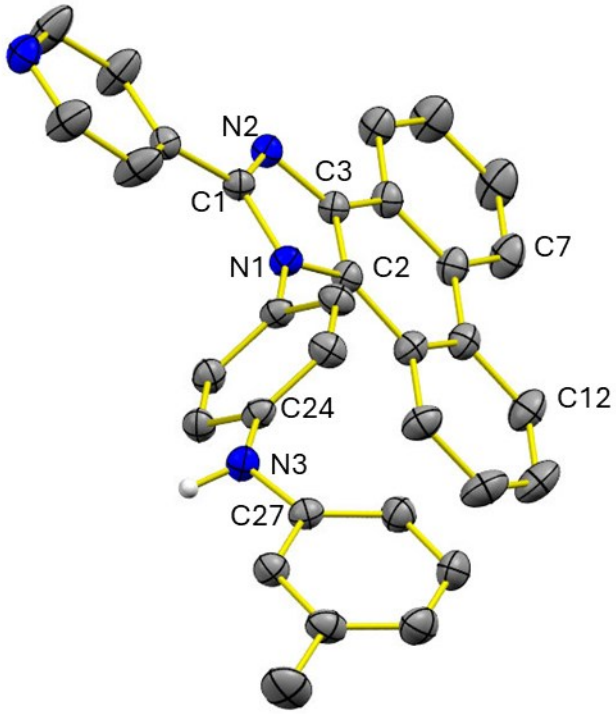

Figure 2. PovRay presentation of PIm-PyTol. Selected hydrogen atoms and the molecule of CH_3CH_2OH were omitted for clarity.

DFT calculations were performed to rationalize the influence of donor architecture on the frontier molecular orbitals of the final divinyl PIm monomers. All calculations were carried out using the Gaussian 16 software package [25] at the B3LYP/6-31+G(d,p) level of theory [26,27], including the GD3BJ empirical dispersion correction [28]. The calculated orbital energy diagram and corresponding orbital distributions are shown in Figure 3. In all three compounds, the HOMO

is mainly localized on the electron-rich donor fragments, confirming that the donor part of the molecule controls the occupied frontier level. This agrees well with the electrochemical data, where the oxidation onset shifts systematically depending on the donor structure. In contrast, the LUMO is located predominantly on the phenanthroimidazole/acceptor-containing fragment, supporting the donor-acceptor nature of the electronic transitions.

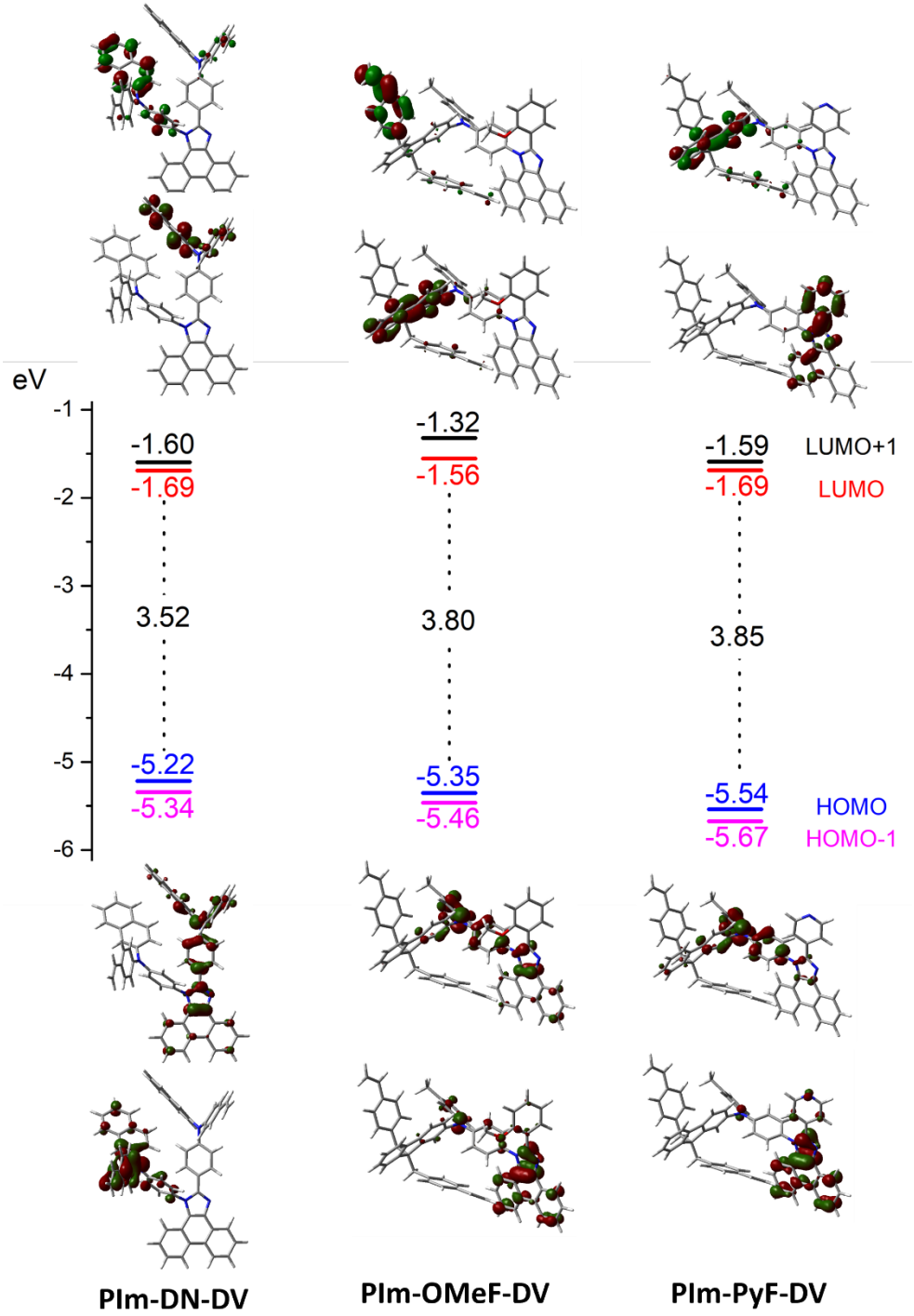

Figure 3. DFT-calculated frontier molecular orbital energy diagram of the divinyl-functionalized phenanthroimidazole monomers PIm-DN-DV, PIm-OMeF-DV, and PIm-PyF-DV. The diagram shows the relative positions of the HOMO, HOMO-1, LUMO, and LUMO+1 levels together with the corresponding molecular orbital distributions. The calculated HOMO levels are mainly associated with the electron-rich donor fragments, whereas the LUMO levels are localized predominantly on the phenanthroimidazole/acceptor-containing part of the molecules, confirming the donor-acceptor character of the designed emitters.

TD-DFT calculations further support the experimentally observed donor-dependent optical trend. The calculated lowest-energy S0→S1 transitions shift from 405 nm for PIm-DN-DV to 380 nm for PIm-OMeF-DV and 368 nm for PIm-PyF-DV, following the same general direction as the experimental optical response. Since the lowest-energy transitions are dominated by HOMO→LUMO excitation, the spatial separation of the frontier orbitals indicates a pronounced intramolecular charge-transfer contribution to the excited state. This orbital distribution is consistent with a mixed excited-state character in which intramolecular charge transfer is superimposed on excitation of the conjugated molecular framework. PIm-DN-DV shows the longest-wavelength calculated transition and the smallest $E_{g(opt)}$ value of 2.73 eV, consistent with the strongest donor contribution and the most extended charge-transfer character within the series [29]. In contrast, the OMeF and PyF derivatives exhibit larger $E_{g(opt)}$ values of 3.08 and 3.12 eV, respectively, in agreement with their more stabilized HOMO levels and blue-shifted calculated transitions. Overall, the combined experimental and theoretical data indicate that donor architecture primarily controls the HOMO energy while modulating the balance between locally excited and charge-transfer contributions to the lowest excited state.

The electronic structure of the final divinyl PIm monomers was investigated by cyclic voltammetry (Fig. 4) and DFT calculations, and the corresponding experimental and calculated parameters are summarized in Table 1. The oxidation onsets shift systematically from 0.38 V for PIm-DN-DV to 0.52 V for PIm-OMeF-DV and 0.62 V for PIm-PyF-DV, giving HOMO(CV) values of -5.18, -5.32, and -5.42 eV, respectively. This trend reflects progressive stabilization of the occupied frontier level upon changing the donor environment from the strongly electron-rich naphthylamine-containing PIm-DN-DV to the fluorene-based OMeF and PyF analogues. The same order is reproduced by DFT, with calculated HOMO levels of -5.22, -5.35, and -5.54 eV for PIm-DN-DV, PIm-OMeF-DV, and PIm-PyF-DV, respectively. The very small difference between HOMO(CV) and HOMO(DFT), particularly for PIm-DN-DV and PIm-OMeF-DV, confirms that the calculations reliably capture the donor-controlled character of the occupied frontier orbitals.

Table 1. Experimental and calculated electronic parameters of the divinyl PIm monomers.

Compound	$E_{ox,\ onset}$, V	HOMO (CV), eV	LUMO*, eV	$E_{g(opt)}$, eV	HOMO (DFT), eV	LUMO (DFT), eV	λ_{ABS} (TD-DFT), nm	Transition	f
PIm-DN-DV	0.38	-5.18	-2.45	2.73	-5.22	-1.69	405	$S_0 \rightarrow S_1$	0.0983

PIm-OMeF-DV	0.52	-5.32	-2.24	3.08	-5.35	-1.56	380	$S_0 \rightarrow S_1$	0.1968
PIm-PyF-DV	0.62	-5.42	-2.30	3.12	-5.54	-1.69	368	$S_0 \rightarrow S_1$	0.1648

*HOMO(CV) values were estimated from oxidation onsets. LUMO values were calculated from HOMO(CV) and $E_{g(opt)}$. $E_{g(opt)}$ was determined from the absorption onset of the UV-Vis spectra. TD-DFT λ_{ABS} values correspond to the calculated lowest-energy S0-S1 transitions.

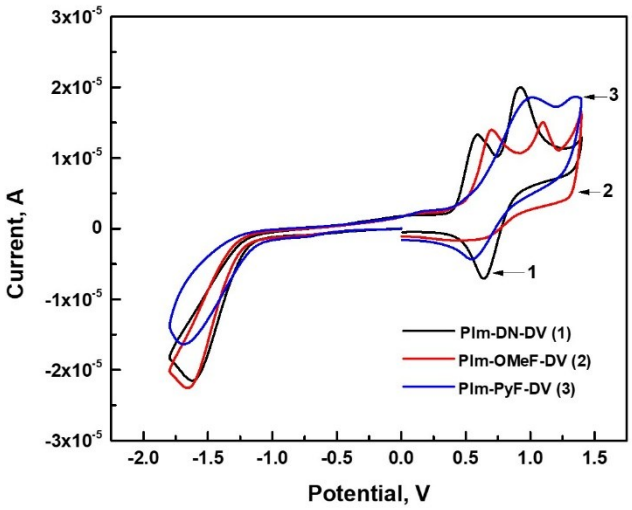

Figure 4. Cyclic voltammograms of PIm-DN-DV, PIm-OMeF-DV, and PIm-PyF-DV recorded in CH_2Cl_2/$TBAPF_6$ using a Pt working electrode and Ag reference electrode. The oxidation onsets shift systematically from PIm-DN-DV to PIm-OMeF-DV and PIm-PyF-DV, reflecting progressive stabilization of the HOMO level.

The LUMO levels estimated from HOMO(CV) and $E_{g(opt)}$ are -2.45, -2.24, and -2.30 eV for PIm-DN-DV, PIm-OMeF-DV, and PIm-PyF-DV, respectively. These values are deeper than the corresponding DFT-calculated LUMO levels, which are located at -1.69, -1.56, and -1.69 eV. This systematic offset is expected because $E_{g(opt)}$ is derived from the absorption onset and therefore reflects the energy of the lowest optical transition rather than a purely ground-state orbital energy difference [30]. In addition, the optical transition includes contributions from intramolecular charge-transfer character and excited-state stabilization, whereas the LUMO (DFT) represents the unoccupied molecular orbital of the optimized ground-state structure. Therefore, the LUMO values estimated using $E_{g(opt)}$ should be treated as approximate experimental energy descriptors, while the most reliable quantitative agreement between experiment and theory is observed for the HOMO levels.

Copolymer formation and thermal properties

The three divinyl-functionalized PIm monomers were copolymerized with *N*-vinylcarbazole under identical free-radical conditions to obtain chromophore-containing VK copolymers suitable for

thin film optical studies. A low chromophore loading of 5 wt.% was selected to suppress excessive chromophore-chromophore interactions while retaining the donor-dependent emissive response of the incorporated PIm units. After precipitation into hexane, the resulting copolymers were isolated as off-white to pale coloured powders in comparable isolated amounts and were processable from chlorinated solvents, enabling the preparation of homogeneous spin-coated films for optical characterization.

The formation of the VK-based copolymers was further supported by ATR-FTIR spectroscopy. Since the PIm-based divinyl monomers were used as minor comonomers at 5 wt.% relative to VK, the most diagnostic spectral changes are associated with the major *N*-vinylcarbazole component [31]. The spectrum of VK contains characteristic vinyl-group bands at approximately 1640, 1365, 1290, and 960 cm^{-1}. After radical copolymerization, these bands disappear in the spectra of all three copolymers, while the dominant aromatic and carbazole-related bands of the PVK-rich matrix are retained. This spectral evolution confirms consumption of the vinyl groups during polymerization and is consistent with the formation of VK-based copolymers containing incorporated PIm chromophore units. The corresponding FTIR spectra are presented in the *Supplementary Information*.

Thermal analysis further confirmed that both the monomers and the resulting VK copolymers possess sufficient thermal robustness for thin film processing and optical studies. Because several monomers exhibit minor preliminary mass-loss events before the principal decomposition step, the onset temperature of the main degradation process (T_{onsMD}) together with T_{max} was used to evaluate the intrinsic thermal stability. The monomers showed distinct degradation behaviours, reflecting their different donor architectures. PIm-DN-DV displayed the highest intrinsic thermal stability in the principal degradation region, with T_{onsMD} and T_{max} values of 512 and 576 °C, respectively, whereas PIm-OMeF-DV and PIm-PyF-DV exhibited lower T_{onsMD} values of 397 and 405 °C and T_{max} values of 431 and 440 °C, respectively. The lower T_5 values observed for PIm-DN-DV and PIm-PyF-DV arise from minor preliminary mass-loss events preceding the principal degradation step and therefore do not reflect the intrinsic thermal stability of the chromophore framework. Accordingly, T_{onsMD} and T_{max} were used as more representative descriptors of intrinsic thermal robustness.

After copolymerization with VK, the pronounced differences observed among the individual monomers became largely suppressed. The copolymers exhibited similar principal degradation behaviour, with T_{onsMD} values in the range of 420-442 °C and nearly identical T_{max} values of 468-471 °C, close to that of pure PVK. This indicates that the thermal degradation of the copolymers is governed predominantly by the PVK matrix, while the incorporated PIm units have only a minor influence on the principal degradation step. Detailed analysis by size exclusion chromatography (SEC) coupled with a multi-angle light scattering (MALS) detector and STA analyses are provided in the *Supplementary Information* and confirm that the obtained materials are polymeric, thermally robust, and suitable for thin film optical studies.

Optical properties of monomers and copolymers

The photophysical properties of the synthesized PIm derivatives were examined in dilute chloroform solutions and in spin-coated films to correlate donor structure with emission behaviour before and after covalent integration into the VK-based polymer matrix. Particular attention was paid to the final divinyl monomers PIm-DN-DV, PIm-OMeF-DV, and PIm-PyF-DV, because these compounds combine donor-tuned phenanthroimidazole emission with terminal vinyl groups suitable for radical copolymerization [32]. The corresponding absorption, excitation, emission, PLQY, and lifetime data are summarized in Table 2.

In dilute chloroform solution, the final monomers exhibit absorption maxima in the near-UV region, with the lowest-energy absorption bands located at 354 nm for PIm-DN-DV, 342 nm for PIm-OMeF-DV, and 347 nm for PIm-PyF-DV (Figure 5, Table 2). The excitation spectra are more sensitive to donor architecture, shifting from 436 nm for PIm-DN-DV to 402 nm for PIm-OMeF-DV and 386 nm for PIm-PyF-DV. The corresponding emission maxima appear at 504, 505, and 484 nm, respectively. Thus, PIm-DN-DV and PIm-OMeF-DV emit in a similar green-blue region, whereas introduction of the pyridyl-substituted PIm fragment in PIm-PyF-DV leads to a noticeable hypsochromic shift [33]. The Stokes shifts remain substantial for all three monomers, particularly for PIm-OMeF-DV and PIm-PyF-DV, indicating pronounced excited-state relaxation and partial charge-transfer character [34,35].

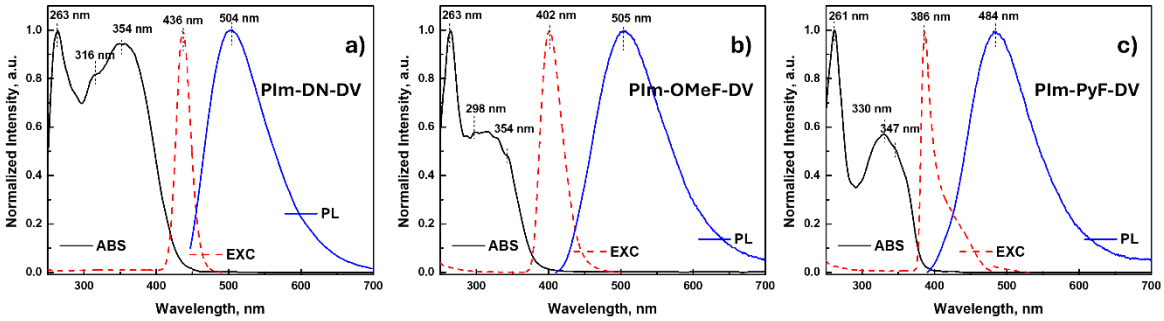

Figure 5. Normalized UV-Vis absorption (black solid line), excitation (red dashed line), and photoluminescence (blue solid line) spectra of PIm-DN-DV, PIm-OMeF-DV, and PIm-PyF-DV recorded in dilute chloroform solution.

The PLQY values further distinguish the final monomers. PIm-DN-DV exhibits moderate emission efficiency in solution with PLQY = 43.3%, whereas PIm-OMeF-DV and PIm-PyF-DV show markedly higher values of 70.6% and 90.1%, respectively. This trend suggests that the fluorene-containing donor architecture, especially in combination with the pyridyl-substituted PIm fragment, favours efficient radiative decay in solution [36, 12].

Time-resolved PL measurements of the final monomers in chloroform reveal nanosecond-scale excited-state decay dynamics (Figure 6a). The decays were fitted using biexponential

functions, giving average lifetimes of 2.40 ns for PIm-DN-DV, 3.28 ns for PIm-OMeF-DV, and 5.20 ns for PIm-PyF-DV. The increase in τ_{avg} across the series follows the increase in emission efficiency and indicates progressively slower excited-state relaxation. The longest lifetime and highest PLQY are observed for PIm-PyF-DV, consistent with the formation of a particularly efficient emissive state in this derivative [37].

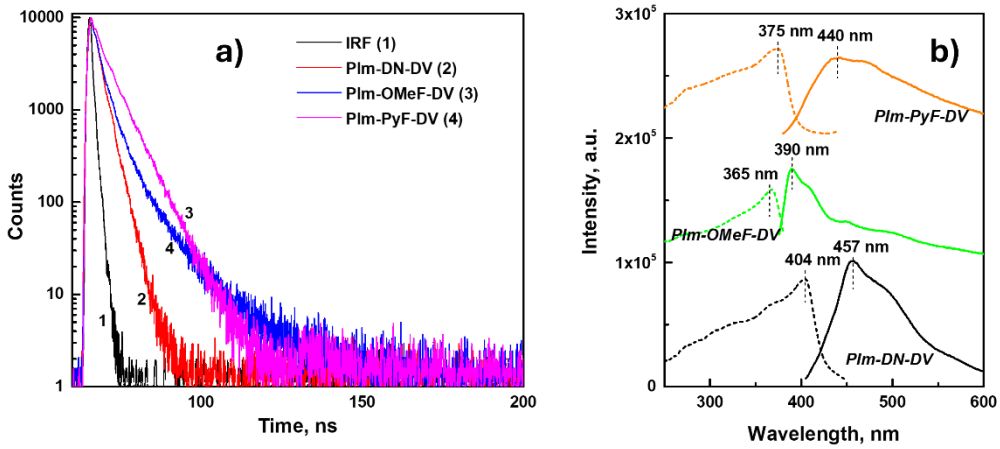

Figure 6. a) Time-resolved photoluminescence (PL) decay curves of PIm-DN-DV (red), PIm-OMeF-DV (blue), and PIm-PyF-DV (magenta) recorded in chloroform solution at room temperature (excitation wavelength: 390 nm; emission monitored at respective PL maxima). The instrument response function (IRF) is shown in black. b) Excitation (dotted lines) and emission (solid lines) spectra of thin films spin-coated from neat chloroform solutions of the three monomers: PIm-DN-DV (black), PIm-OMeF-DV (green), and PIm-PyF-DV (orange). All spectra were measured at room temperature under ambient conditions.

In neat spin-coated films, all three divinyl monomers exhibit pronounced hypsochromic shifts of both excitation and emission maxima compared with their solution spectra (Figure 6b, Table 2). The emission maxima shift from 504 to 457 nm for PIm-DN-DV, from 505 to 390 nm for PIm-OMeF-DV, and from 484 to 440 nm for PIm-PyF-DV. This blue shift indicates that the solid-state environment suppresses the relaxed low-energy emissive states observed in solution, most likely through restricted conformational relaxation and altered intermolecular packing [38,39]. The effect becomes even more pronounced after covalent incorporation into the VK-based matrix. The copolymer films show nearly identical absorption maxima at 343 nm and closely similar E_g values of 3.38-3.43 eV, indicating that their ground-state optical response is largely dominated by the carbazole-rich matrix with contribution from the embedded PIm chromophores (Figure 7a, Table 2). In contrast, their emission remains donor-dependent: Poly(PIm-OMeF-DV-co-VK) emits at 386 nm, Poly(PIm-PyF-DV-co-VK) at 406 nm, and Poly(PIm-DN-DV-co-VK) at 428 nm. Thus, the VK matrix largely levels the absorption characteristics while preserving donor-controlled excited-state emission [40].

Table 2. Photophysical properties of the synthesized intermediates, divinyl monomers, and VK copolymer films. The data include absorption (λ_{ABS}), excitation (λ_{exc}), and emission (λ_{em}) maxima, Stokes shift ($\Delta\lambda$), optical bandgaps (E_g), photoluminescence quantum yields (PLQY), and average lifetimes (τ_{avg}). Solution data were measured in dilute chloroform at room temperature, whereas copolymer data refer to spin-coated films.

Compound	λ_{ABS}, nm	λ_{exc}, nm	λ_{em}, nm	Stokes shifts, nm	E_g^*, eV	PLQY, %	τ_{avg}, ns
PIm-Br	359	370	387	17	3.30	-	1.02
PIm-DN	356	428	504	76	2.85	-	1.17
PIm-DN-DV	354	436	504	68	2.73	43.3	2.40
Poly(PIm-DN-DV-*co*-VK)-films	343	348	428	80	3.42	49.5	1.93
PIm-BrOMe	356	363	382	19	3.36	-	4.07
PIm-OMeTol	357	362	383	21	3.37	-	3.98
PIm-OMeF-DV	342	402	505	103	3.08	70.6	3.28
Poly(PIm-OMeF-DV-*co*-VK)-films	343	341	386	45	3.38	90.8	1.37
PIm-BrPy	359	424	480	56	3.23	-	2.03
PIm-PyTol	363	381	405	24	3.16	-	6.96
PIm-PyF-DV	347	386	484	98	3.12	90.1	5.20
Poly(PIm-PyF-DV-*co*-VK)-films	343	342	406	64	3.43	92.4	1.36

* E_g values were determined from the absorption onset using the tangent method. PLQY values were measured for the final divinyl monomers in solution and for the copolymer films.

Most importantly, covalent incorporation into the VK-based matrix gives highly efficient solid-state emission for the fluorene-containing copolymers. Poly(PIm-OMeF-DV-co-VK) and Poly(PIm-PyF-DV-co-VK) exhibit PLQY values of 90.8% and 92.4%, respectively, exceeding or retaining the high efficiencies of the corresponding monomers [41,42]. In contrast, the DN-containing copolymer shows a lower but still significant PLQY of 49.5%. These results indicate that the VK matrix provides a favourable environment for maintaining efficient emission from the incorporated chromophores, particularly for the OMeF and PyF derivatives.

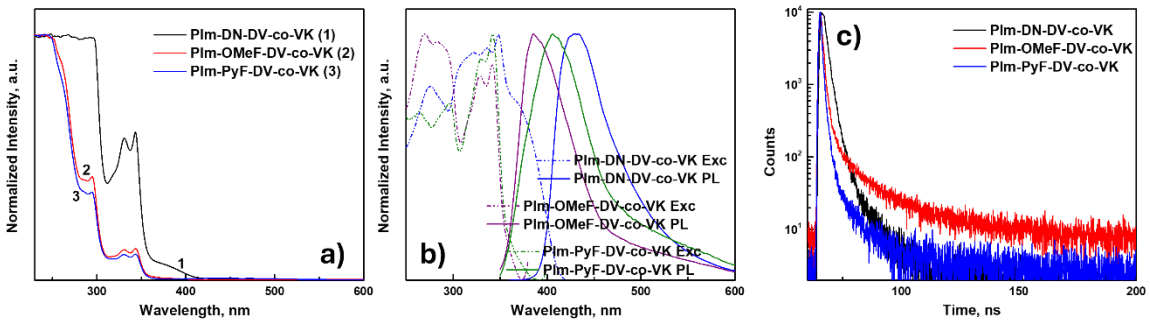

Figure 7. (a) UV-Vis absorption spectra of spin-coated films of the copolymers PIm-DN-DV-*co*-VK, PIm-OMeF-DV-*co*-VK, and PIm-PyF-DV-*co*-PVK on glass; (b) Normalized excitation (dashed) and PL

(solid) spectra of the same films measured under identical conditions; (c) Time-resolved PL decays of the copolymer films monitored at their respective PL maxima (λ_{exc}=390 nm); the instrument response function (IRF) is shown in black. All measurements were performed at room temperature; spectra were baseline-corrected and normalized.

The time-resolved PL decays of the copolymer films are single-exponential and faster than those of the corresponding monomers in solution, with τ_{avg} values of 1.93 ns for Poly(PIm-DN-DV-co-VK), 1.37 ns for Poly(PIm-OMeF-DV-co-VK), and 1.36 ns for Poly(PIm-PyF-DV-co-VK) (Figure 7c). The preservation of distinct donor-dependent emission maxima despite the convergence of the absorption profiles indicates that the emissive response remains predominantly associated with the incorporated PIm chromophores rather than being determined solely by the VK-rich matrix. At the same time, the pronounced blue shifts relative to the corresponding monomers in solution, and the shorter, single-exponential lifetimes show that covalent incorporation into the polymer substantially modifies excited-state relaxation. Thus, the copolymer emission can be described as chromophore-associated but strongly modulated by the local carbazole-rich environment.

Conclusions

Three divinyl-functionalized phenanthro[9,10-*d*]imidazole emitters, PIm-DN-DV, PIm-OMeF-DV, and PIm-PyF-DV, were designed and synthesized as donor-tunable molecular fluorophores and polymerizable building blocks for emissive VK-based copolymers. The synthetic strategy enabled the introduction of distinct donor fragments together with terminal vinyl groups suitable for radical copolymerization. Structural analysis, NMR spectroscopy, and elemental analysis confirmed the formation of the designed intermediates and final monomers.

The combined experimental and computational data show that donor architecture governs the electronic and photophysical behaviour of the series. The final monomers exhibit donor-dependent emission in solution, with PLQY values increasing from 43.3% for PIm-DN-DV to 70.6% for PIm-OMeF-DV and 90.1% for PIm-PyF-DV. This trend supports the favourable role of the fluorene-containing donor architecture, particularly in the pyridyl-substituted derivative, in promoting efficient radiative decay.

Copolymerization with *N*-vinylcarbazole provided processable VK-based materials in which the PIm chromophores are covalently embedded at low loading. In the resulting films, absorption is largely defined by the carbazole-rich matrix, whereas emission remains controlled by the incorporated PIm units. The copolymer films show violet-to-blue emission with maxima between 386 and 428 nm and fast nanosecond decay dynamics. Most importantly, the fluorene-containing copolymers display very high solid-state PLQY values of 90.8% and 92.4%, confirming that the VK matrix provides an efficient environment for preserving bright emission in the solid state.

Overall, this study demonstrates that divinyl-functionalized phenanthroimidazoles are promising polymerizable emitters for the preparation of bright, donor-tunable luminescent

polymer films. The combination of modular synthesis, covalent polymer integration, high thermal robustness, and significant solid-state emission efficiency makes this molecular platform attractive for further development of functional emissive materials.

Author contributions

Liudmila Loghina: writing - original draft, supervision, methodology, investigation, formal analysis, data curation, and conceptualization. Jiri Jancalek, Zuzana Zmrhalova, Roman Jambor, Ales Imramovsky, Stepan Podzimek, Zdena Ruzickova and Miroslav Vlcek: formal analysis, data curation, visualization, and writing - review and editing. Roman Jambor, Miroslav Vlcek: supervision and project administration.

Conflicts of interest

There are no conflicts to declare.

Data availability

All supporting data are included in the article and its SI. Detailed experimental sections, NMR and FTIR spectroscopy, TGA data, and characterization. See DOI: ///

The datasets generated during and/or analysed during the current study are available in the Figshare repository, DOI: 10.6084/m9.figshare.33102008.

Acknowledgments

This work has been funded by a grant from the Programme Johannes Amos Comenius under the Ministry of Education, Youth and Sports of the Czech Republic [No. CZ.02.01.01/00/23_021/0008593], and by a grant LM2023037 from the Ministry of Education, Youth and Sports of the Czech Republic.

References

[1] Breul A. M., Hager M. D., Schubert U. S., 2013. Fluorescent monomers as building blocks for dye labeled polymers: synthesis and application in energy conversion, biolabeling and sensors. Chem. Soc. Rev. 42 (12), 5366–5407. https://doi.org/10.1039/c3cs35478d.

[2] Ahumada G., Borkowska M., 2022. Fluorescent polymers conspectus. Polymers 14 (6), 1118. https://doi.org/10.3390/polym14061118.

[3] Ye S., BaoY., 2024. Recent advances in fluorescent polymers with color-tunable aggregate emission. Chem. Mater., 36 (12), 5878–5896. https://doi.org/10.1021/acs.chemmater.3c02714.

[4] Plouzeau M., Piogé S., Peilleron F., Fontaine L., Pascual S., 2022. Polymer/dye blends: preparation and optical performance: a short review. J. Appl. Polym. Sci. 139 (36), e52861. https://doi.org/10.1002/app.52861.

[5] Reisch, A., Klymchenko, A.S., 2016. Fluorescent polymer nanoparticles based on dyes: seeking brighter tools for bioimaging. Small 12, 1968-1992. https://doi.org/10.1002/smll.201503396.

[6] Kar M., Mandal T. K., 2024. End-/side-chain fluorescent polymer conjugates: Stimuli-responsiveness and biological applications. J. Polym. Sci. 62(6), 1074-1114. https://doi.org/10.1002/pol.20230584.

[7] Tatsi E., Ragno G.R., Nitti A. *et al*., 2025. Tailoring aggregation-induced emission in luminescent solar concentrators through controlled polymerization. Commun Chem 8, 312. https://doi.org/10.1038/s42004-025-01700-1.

[8] Bao Y., 2024. Polymerization-mediated through-space charge transfer: An emerging strategy for light-emitting materials. Langmuir 40 (7), 3275-3282. https://doi.org/10.1021/acs.langmuir.3c03376.

[9] Tagare J., Vaidyanathan S., 2018. Recent development of phenanthroimidazole-based fluorophores for blue organic light-emitting diodes (OLEDs): an overview. J. Mater. Chem. C 6 (38), 10138-10173. https://doi.org/10.1039/c8tc03689f.

[10] Szlapa-Kula, A., Kula, S., 2023. Progress on phenanthroimidazole derivatives for light-emitting electrochemical cells: An Overview. Energies 16, 5194. https://doi.org/10.3390/en16135194.

[11] Debata B. P., Patel S., Vaidyanathan S., 2026. Fluorophores with imidazole building blocks and their multifunctional platforms for optoelectronics (LEDs/OLEDs), chemo-sensing, and security applications: recent advances and future perspectives. J. Mater. Chem. C 14(13), 5141-5176. https://doi.org/10.1039/d5tc03845f.

[12] Wang Y., Du C., Cheng Z., Ge S., Feng Z., Wan L., Hu Y., Ma X., Su Z., Lu P., 2024. Rational molecular design of phenanthroimidazole-based fluorescent materials toward high-efficiency deep-blue OLEDs by molecular isomer engineering. ACS Appl. Mater. Interfaces 16(38), 51201-51211. https://doi.org/10.1021/acsami.4c05510.

[13] Jayabharathi J., Panimozhi S., Thanikachalam V., 2019. Asymmetrically twisted phenanthrimidazole derivatives as host materials for blue fluorescent, green and red phosphorescent OLEDs. Sci Rep 9, 17555. https://doi.org/10.1038/s41598-019-54125-x.

[14] Li Z., Lu J., Li S., Qin S., Qin Y., 2012. Orderly ultrathin films based on perylene/Poly(N-vinyl carbazole) assembled with layered double hydroxide nanosheets: 2D fluorescence resonance

energy transfer and reversible fluorescence response for volatile organic compounds. Adv. Mater. 24, 6053-6057. https://doi.org/10.1002/adma.201203040.

[15] Aoki H., Takahashi T., Tamai Y. *et al.*, 2009. Poly(methacrylate)s labeled by perylene diimide: synthesis and applications in single chain detection studies. Polym J 41, 778-783. https://doi.org/10.1295/polymj.PJ2009099.

[16] Butkute R., Peciulyte L., Lygaitis R., Buika G., Gudeika D., 2018. Synthesis and properties of vinyl-functionalized phenanthroimidazole-based self-polymerizable monomers. Molecular Crystals and Liquid Crystals 670(1), 134-146. https://doi.org/10.1080/15421406.2018.1542073.

[17] Butkute R., Peciulyte L., Lygaitis R. *et al.*, 2019. Phenanthroimidazole-based monomers: synthesis, properties and self-polymerization. Polym. Bull. 76, 153-174. https://doi.org/10.1007/s00289-018-2373-3.

[18] Loghina L., Machotova J., Svoboda R., Houdek J., Kohl M., Ruzickova Z., Jambor R., Vlcek M., 2025. Photoluminescent phenanthroimidazole derivatives as covalently linked UV stabilizers for latex coatings. RSC Adv. 15(35), 28827-28840. https://doi.org/10.1039/d5ra05109f.

[19] Grazulevicius J.V., Strohriegl P., Pielichowski J., Pielichowski K., 2003. Carbazole-containing polymers: synthesis, properties and applications. Progress in Polymer Science 28(9), 1297-1353. https://doi.org/10.1016/S0079-6700(03)00036-4.

[20] Geffroy C., Grana E., Mumtaz M., Cojocaru L., Cloutet E., Olivier C., Uchida S., Toupance T., Segawa H., Hadziioannou G., 2019. Post-functionalization of polyvinylcarbazoles: An open route towards hole transporting materials for perovskite solar cells. Solar Energy 193, 878-884. https://doi.org/10.1016/j.solener.2019.10.034.

[21] Kothavale S., Bhalekar S., Sekar N., 2018. Highly fluorescent blue-green emitting phenanthroimidazole derivatives: Detail experimental and DFT study of structural and donating group effects on fluorescence properties. Dyes and Pigments 159, 209-221. https://doi.org/10.1016/j.dyepig.2018.06.020.

[22] Kula S., Ledwon P., Maroń A. M., Siwy M., Grzelak J., Szalkowski M., Maćkowski S., Schab-Balcerzak E., 2021. Synthesis, photophysical properties and electroluminescence characterization of 1-phenyl-1H-phenanthro[9,10-d]imidazole derivatives with N-donor substituents. Dyes and Pigments 192, 109437. https://doi.org/10.1016/j.dyepig.2021.109437.

[23] Dorel R., Grugel C. P., Haydl A. M., 2019. The Buchwald–Hartwig amination after 25 years. Angew. Chem. Int. Ed. 58, 17118-17129. https://doi.org/10.1002/anie.201904795.

[24] Bosiak M. J., Zielińska A. A., Trzaska P., Kędziera D., Adams J., 2021. Buchwald–Hartwig amination of aryl halides with heterocyclic amines in the synthesis of highly fluorescent

benzodifuran-based star-shaped organic semiconductors. J. Org. Chem. 86(24), 17594-17605. https://doi.org/10.1021/acs.joc.1c01583.

[25] Frisch M. J., Trucks G. W., Schlegel H. B., *et al*., 2016. Gaussian 16, Revision A.03M, Gaussian, Inc., Wallingford, CT.

[26] Becke A. D., 1993. Density-functional thermochemistry. III. The role of exact exchange. J. Chem. Phys. 98, 5648-5652. https://doi.org/10.1063/1.464913.

[27] Lee C., Yang W., Parr R. G., 1988. Development of the Colle-Salvetti correlation-energy formula into a functional of the electron density. Phys. Rev. B 37, 785-789. https://doi.org/10.1103/PhysRevB.37.785.

[28] Grimme S., Ehrlich S., Goerigk L., 2011. Effect of the damping function in dispersion corrected density functional theory. J. Comput. Chem. 32, 1456-1465. https://doi.org/10.1002/jcc.21759.

[29] Rout Y., Montanari C., Pasciucco E., Misra R., Carlotti B., 2021. Tuning the fluorescence and the intramolecular charge transfer of phenothiazine dipolar and quadrupolar derivatives by oxygen functionalization. J. Am. Chem. Soc. 143(26), 9933-9943. https://doi.org/10.1021/jacs.1c04173.

[30] Djurovich P. I., Mayo E. I., Forrest S. P., Thompson M. E., 2009. Measurement of the lowest unoccupied molecular orbital energies of molecular organic semiconductors, Organic Electronics 10(3), 515-520. https://doi.org/10.1016/j.orgel.2008.12.011.

[31] Al Lafi A. G., Hay J. N., 2019. 2D-COS-FTIR analysis of high molecular weight poly (N-vinyl carbazole) undergoing phase separation on purification and thermal annealing. J. Mol. Struct. 1175, 152-162. https://doi.org/10.1016/j.molstruc.2018.07.077.

[32] Brar A. S., Kaur M., Balamurli M. M., Dogra S. K., 2006. Photophysical studies of copolymers of N-vinylcarbazole. J. Appl. Polym. Sci. 100, 372-380. https://doi.org/10.1002/app.23183.

[33] Krawczyk P., Czeleń P., Cysewski P., 2018. Reactive group effects on the photophysical and biological properties of 2-phenyl-1H-phenanthro[9,10-d]imidazole derivatives as fluorescent markers. Org. Biomol. Chem. 16(20), 3788-3800. https://doi.org/10.1039/c8ob00729b.

[34] Aderne R. E., Borges B. G. A. L., Ávila H. C., Kieseritzky F., Hellberg J., *et al.*, 2022. On the energy gap determination of organic optoelectronic materials: the case of porphyrin derivatives. Mater. Adv. 3(3), 1791-1803. https://doi.org/10.1039/d1ma00652e.

[35] Wu S., Ban Z., Tang H., Ma N., Ran X., *et al.*, 2025. Large Stokes shift by increasing intramolecular charge transfer for high signal-to-background ratio bioimaging. Chem. Commun. 61(57), 10574-10577. https://doi.org/10.1039/d5cc02608c.

[36] Jayabharathi J., Sathishkumar R., Thanikachalam V., 2014. Organic light-emitting materials based on iridium(III) complexes bearing phenanthroimidazole ligands. J. Phys. Org. Chem. 27(6), 504-511. https://doi.org/10.1002/poc.3292.

[37] Sharma A., Thomas K. R. J., Nagar M. R., Jou J.-H., 2021. Phenanthroimidazole-based bipolar carbazoles featuring cyano substituents to realize efficient deep-blue electroluminescence with an external quantum efficiency of nearly 6%. Mater. Adv. 2(19), 6326-6338. https://doi.org/10.1039/d1ma00604e.

[38] Congrave D. G., Drummond B. H., Gray V., Bond A. D., Rao A., Friend R. H., Bronstein H., 2021. Suppressing aggregation induced quenching in anthracene based conjugated polymers. Polym. Chem. 12(12), 1830-1836. https://doi.org/10.1039/d1py00118c.

[39] Kim H., Kwak G., 2024. Fluorescent polyimide films with covalently incorporated perylenediimide. ACS Appl. Polym. Mater. 6(12), 7311-7319. https://doi.org/10.1021/acsapm.4c01308.

[40] Li P., Zhang D., Zhang Y., Lu W., Zhang J., Wang W., *et al*., 2019. Aggregation-caused quenching-type naphthalimide fluorophores grafted and ionized in a 3D polymeric hydrogel network for highly fluorescent and locally tunable emission. ACS Macro Lett. 8(8), 937-942. https://doi.org/10.1021/acsmacrolett.9b00337.

[41] Jayabharathi J., Nethaji P., Thanikachalam V., Ramya R., 2019. Derivatives of cyanonaphthyl-substituted phenanthroimidazole as blue emitters for nondoped organic light-emitting diodes. ACS Omega 4(3), 4553-4570. https://doi.org/10.1021/acsomega.8b03617.

[42] Sharma A., Thomas K. R. J., Kesavan K. K., Siddiqui I., Nagar M. R., Jou J.-H., 2021. Effect of cyano on the functional properties of phenanthroimidazole-substituted carbazole derivatives. ACS Appl. Electron. Mater. 3(9), 3876-3888. https://doi.org/10.1021/acsaelm.1c00482.